

Probing Cosmic Neutrino Background through Parametric Fluorescence

Guo-yuan Huang^{1,*} and Shun Zhou^{2,3,†}

¹*School of Mathematics and Physics, China University of Geosciences, 430074 Wuhan, China*

²*Institute of High Energy Physics, Chinese Academy of Sciences, Beijing 100049, China*

³*School of Physical Sciences, University of Chinese Academy of Sciences, Beijing 100049, China*

(Dated: July 16, 2025)

We point out that relic neutrinos from the Big Bang may induce the parametric fluorescence in molecular systems, which offers a novel way to discover cosmic neutrino background. By coherently scattering with molecular energy levels, a massive neutrino can spontaneously “decay” into a lighter neutrino and an infrared signal photon, i.e., $\nu_i + M \rightarrow \nu_j + \gamma_s + M$, where the molecular state M remains unchanged after the scattering. Because the amplitudes of different radiants are matched in phase, the rate is coherently enhanced and proportional to the squared density of ambient dipoles. When the energy transfer from neutrinos coincides with the molecular energy-level difference, the fluorescence will be on resonance. We find that the event rate for $\nu_i \rightarrow \nu_j + \gamma_s$ at the resonance peak through the magnetic dipole transition can reach $R \sim 5 \text{ yr}^{-1}$ (or 10 yr^{-1}) for Dirac (or Majorana) neutrinos for a nominal target with a spatial dimension of $l = 3 \text{ m}$. Parity mixing by the Stark effect may help to further magnify the signal rate.

I. INTRODUCTION

The Big Bang theory predicts the existence of both cosmic microwave background (CMB) and cosmic neutrino background (CνB). While the CMB has been firmly observed and serves as a powerful probe of the early Universe [1], the CνB, formed one second after the Big Bang, has yet to be detected. To date, the most promising method for observing these relic neutrinos is through the inverse beta-decay process, initially proposed by S. Weinberg in 1962 [2]. Nevertheless, the PTOLEMY project, currently under development with tritium targets, still faces significant challenges before its practical feasibility can be confirmed [3–7]. An alternative approach to relic neutrino detection is to observe the mechanical recoils from their coherent scattering on a macroscopic object [8–25]. However, while the event rate for coherent scattering can be enhanced by a factor of the Avogadro constant $N_A \approx 6.02 \times 10^{23}$, the resulting sub-eV recoil is averaged across all the atoms in the target ensemble, posing a fundamental challenge for detecting those elusive relics.

In this work, we investigate a novel phenomenon of the coherent parametric fluorescence of relic neutrinos in cold molecular (or atomic) systems. A schematic plot for the process is shown in the left panel of Fig. 1. By collectively interacting with molecular dipoles, the parametric fluorescence $\nu_i + M \rightarrow \nu_j + \gamma_s + M$ with neutrino masses $m_i > m_j$ will be induced, a spontaneous process that is unlikely to occur without the presence of the medium. Microscopically, neutrinos are scattering with dipoles in the medium through their coupling to electrons, and the process is coherent for the ensemble because dipoles in the medium remain unmodified after the scattering.

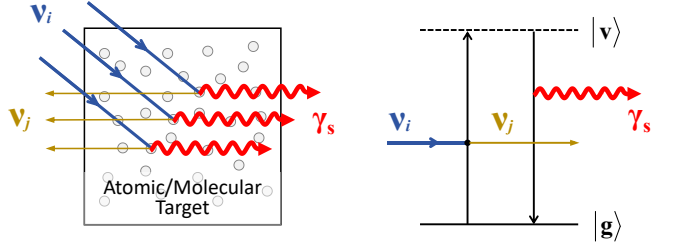


FIG. 1. Schematic diagrams for the parametric fluorescence induced by massive neutrinos, which collectively interact with molecular (or atomic) dipoles in the medium.

The medium of our concern is characterized by generic electric or magnetic dipoles \mathbf{d} of Avogadro’s number. Those dipoles radiate collectively if the phases of their scattering amplitudes are matched. The microscopic process of the parametric fluorescence is described by the diagram on the right panel of Fig. 1. We assume that all the molecules in the system are in their ground state $|g\rangle$, by maintaining a low medium temperature. Neutrino fields couple to the dipole system via the four-fermion interaction, while photons couple to the system via the electric (or magnetic) dipole interaction $\mathbf{d} \cdot \mathbf{E}$ (or $\mathbf{d} \cdot \mathbf{B}$). When a heavier relic neutrino ν_i passes through this medium, it can first excite the dipole to a virtual state $|v\rangle$ and be converted to a lighter neutrino ν_j . The virtual energy level is off-shell and quickly jumps back to the ground state by radiating a photon γ_s . If the scattering amplitude contributed by each radiant of the medium is represented by \mathcal{M}_r , then the total amplitude of scattered waves will be

$$\mathcal{M}_{\text{tot}} = \sum_{r=1}^N \mathcal{M}_r \cdot e^{i(\mathbf{p}_i - \mathbf{p}'_j - \mathbf{k}) \cdot \mathbf{x}_r}. \quad (1)$$

Here, N refers to the total number of dipoles in the medium, \mathbf{x}_r is the position of the dipole radiant \mathbf{d}_r , and \mathbf{p}_i , \mathbf{p}'_j and \mathbf{k} are the momenta of the initial neutrino, the

* huanguoyuan@cug.edu.cn

† zhoush@ihep.ac.cn

outgoing neutrino and the signal photon, respectively. When the phase matching condition $\mathbf{q} \equiv \mathbf{p}_i - \mathbf{p}'_j - \mathbf{k} = 0$ is satisfied (for a uniform medium), different dipoles will radiate in phase and the event rate will receive an N^2 enhancement. This is also in line with the picture of coherent forward scatterings of neutrinos, which modifies the neutrino dispersion relation in medium.

Since there is no energy transfer from the incident neutrino to the medium ultimately, the kinematics for the process $\nu_i \rightarrow \nu_j + \gamma_S$ is similar to radiative neutrino decays in vacuum. The neutrino mass ordering, which will be determined within a few years by JUNO [26, 27], affects the energy of the signal photon. For concreteness, we take the lightest neutrino mass to be vanishing, and thus the heaviest neutrino mass will be $m \approx 0.05$ eV. In the case of normal mass ordering (NO), the heaviest neutrino will be ν_3 , and the photon energy for $\nu_3 \rightarrow \nu_1$ or ν_2 should be about $\omega \sim 0.025$ eV, which falls within the far-infrared range of light. In the case of inverted mass ordering (IO), the transition from the heaviest neutrino will generate a photon with energy about $\omega \sim 0.025$ eV (for $\nu_2 \rightarrow \nu_3$) or $\omega \sim 7.5 \times 10^{-4}$ eV (for $\nu_2 \rightarrow \nu_1$), the latter of which corresponds to the microwave frequency. Therefore, we shall focus on two representative scenarios: $\nu_3 \rightarrow \nu_1$ in the NO case and $\nu_2 \rightarrow \nu_1$ in the IO case. While it might be challenging to detect single quantum of microwave, one-photon detection at far-infrared frequencies should be feasible with modern or near-future technologies [28], such as superconducting tunnel junction sensors [29], kinetic inductance detectors [30], quantum capacitance detectors [31], etc. For simplicity, we further assume that the transportation of light to the sensor through the medium is non-dissipative.

In nonlinear optics, a laser beam γ_P pumping into certain crystals can be efficiently converted into two photon beams γ_S and γ_I at lower energies by coherently scattering with the energy levels of dipoles in the crystal. This process $\gamma_P \rightarrow \gamma_S + \gamma_I$ is referred to as the spontaneous parametric down-conversion (SPDC) [32–35], arising from the nonlinear electric susceptibility of the material. The coherence requirement leads to a similar phase matching condition, i.e., $\mathbf{k}_P = \mathbf{k}_S + \mathbf{k}_I$, along with the energy conservation. The conversion efficiency relies largely on the detailed configurations of molecules, and can be calculated from first principles of quantum mechanics. The most intriguing aspect of this well-established phenomenon is that resonance enhancement occurs when the frequency of the radiation aligns with the corresponding energy-level difference [32, 33]. The fluorescence process induced by neutrinos is similar to the pure electromagnetic scenario. This phenomenon should be distinguished from the very soft photon emission due to coherent scattering of neutrinos with free electron gas [16].

In the remaining part, we first derive the effective Hamiltonian for the neutrino-photon interaction in the presence of molecular dipoles, and then estimate event rates for the parametric fluorescence of relic neutrinos.

In the end, we briefly comment on possible mechanisms for additional enhancement and conclude.

II. PARAMETRIC FLUORESCENCE OF MASSIVE NEUTRINOS IN MEDIUM

The fluorescence processes can be interpreted as the dipole radiation of a polarized medium under the perturbation of external fields. As shown in the right panel of Fig. 1, the essence is to have a two-level system with a ground state $|g\rangle$ and a virtual state $|v\rangle$. The system is initially prepared in the ground state $|g\rangle$. Through the virtual state $|v\rangle$, the scattering process then reads $\nu_i + |g\rangle \rightarrow \nu_j + |g\rangle + \gamma$. Diagrammatically, the initial neutrino first strikes the ground state to the virtual state through the four-fermion weak interaction, inducing a collective dipole polarization in the medium. According to the uncertainty principle, this virtual state is highly unstable and quickly returns to the ground state by emitting a photon via the electromagnetic coupling. There is of course another diagram where the ground state first transits to the virtual state by emitting a photon, and then absorbs the energy from the neutrino scattering. Nevertheless, it is easy to verify that the amplitude is dominated by the diagram shown in Fig. 1, for which the virtual state is more on-shell. Furthermore, the scattering amplitude in principle receives contributions from many possible discrete intermediate states rather than only one state $|v\rangle$ in the diagram, but one of those intermediate states close to the resonance will be dominant, as we will show later.

To compute the event rate, we first write down the four-fermion coupling for the non-diagonal transition of neutrinos,

$$-\mathcal{L} \supset \sum_{i,j=1}^3 \frac{G_F C_{ij}}{\sqrt{2}} \bar{\nu}_j \gamma^\mu (1 - \gamma_5) \nu_i \cdot \bar{e} \gamma_\mu (1 - \gamma_5) e, \quad (2)$$

where G_F is the Fermi constant and $C_{ij} \equiv U_{ei}^* U_{ej}$ ($i \neq j$) with U being the Pontecorvo-Maki-Nakagawa-Sakata (PMNS) matrix. The above Lagrangian can be simplified due to the following two facts: (i) electrons are non-relativistic in atoms; (ii) for an efficient electromagnetic transition from $|v\rangle$ to $|g\rangle$, the electron current should be chosen to be of either E1 or M1 type. Thus, we identify two relevant parts, i.e., the temporal term of the vector current $\bar{e} \gamma_0 e$ and the spatial term of the axial-vector current $\bar{e} \gamma_5 e$.

The temporal term $\bar{e} \gamma_0 e$ will lead to the E1-type transition. To clarify this, we denote the electron wavefunctions for the ground and virtual states as Ψ_g and Ψ_v , respectively. The transition matrix $\langle v | H | g \rangle$ will be proportional to $\int d^3 \mathbf{x} \Psi_v^*(\mathbf{x}) \Psi_g(\mathbf{x}) \exp[i(\mathbf{p}_i - \mathbf{p}'_j) \cdot \mathbf{x}]$, where the spatial phase factor comes from the neutrino field decomposition. Expanding the phase factor, the first non-vanishing term is $i \int d^3 \mathbf{x} \Psi_v^*(\mathbf{x}) \Psi_g(\mathbf{x}) \cdot (\mathbf{p}_i - \mathbf{p}'_j) = i \mathbf{x}_{vg} \cdot (\mathbf{p}_i - \mathbf{p}'_j)$, which just represents the E1-type transition with $\mathbf{x}_{vg} \equiv \langle v | \mathbf{x} | g \rangle$. The usual electric dipole

moment is defined as $\mathbf{d}_{\text{vg}} \equiv -e \mathbf{x}_{\text{vg}}$.

The spatial term $\bar{e}\gamma\gamma_5 e$, recast as $\langle \mathbf{v} | \boldsymbol{\sigma} | \mathbf{g} \rangle \equiv -\boldsymbol{\sigma}_{\text{vg}}$ in the non-relativistic limit, gives rise to a spin-flipped transition that belongs to the M1 type. Note that the matrix element for the M1-type transition induced by neutrinos is of order one. In comparison, the E1-type transition for neutrinos is limited by the Bohr radius

$a_0 = 1/(\alpha m_e)$, which brings in a suppression factor $m_i^2 a_0^2 \sim 10^{-10}$ in rates compared to the M1 type.

On the basis of atomic energy eigenstates, the effective Hamiltonian per dipole in the interaction picture, describing the coupling of fields in the momentum space, turns out to be

$$-H_I^{\text{E1}}(t, \mathbf{x}_d) = \frac{G_F C_{ij}}{\sqrt{2}i} \hat{j}_{ij}^0(\mathbf{p}_i, \mathbf{p}'_j) \mathbf{x}_{\text{vg}} \cdot (\mathbf{p}_i - \mathbf{p}'_j) e^{i(E_{\text{vg}} + E'_j - E_i)t} |\mathbf{v}\rangle \langle \mathbf{g}| + \mathbf{d}_{\text{vg}} \cdot \boldsymbol{\mathcal{E}}(\mathbf{k}) e^{i(-E_{\text{vg}} + \omega)t} |\mathbf{g}\rangle \langle \mathbf{v}| + \text{h.c.}, \quad (3)$$

$$-H_I^{\text{M1}}(t, \mathbf{x}_d) = \frac{G_F C_{ij}}{\sqrt{2}} \hat{\mathbf{j}}_{ij}(\mathbf{p}_i, \mathbf{p}'_j) \cdot \boldsymbol{\sigma}_{\text{vg}} e^{i(E_{\text{vg}} + E'_j - E_i)t} |\mathbf{v}\rangle \langle \mathbf{g}| + \mathbf{d}_{\text{vg}} \cdot \boldsymbol{\mathcal{B}}(\mathbf{k}) e^{i(-E_{\text{vg}} + \omega)t} |\mathbf{g}\rangle \langle \mathbf{v}| + \text{h.c.}, \quad (4)$$

for the E1-type and M1-type interactions, respectively, where E_{vg} denotes the energy difference between $|\mathbf{v}\rangle$ and $|\mathbf{g}\rangle$, and we recall that ω represents the photon energy. For notation convenience, we have assumed that the momentum modes are discrete, which does not affect the ultimate results. The contributing neutrino current operator in the momentum space is given by

$$\hat{j}_{ij}^\mu = \bar{\nu}_{\mathbf{p}'_j}^{(+)} \gamma^\mu (1 - \gamma_5) \nu_{\mathbf{p}_i}^{(-)} + \bar{\nu}_{\mathbf{p}_i}^{(-)} \gamma^\mu (1 - \gamma_5) \nu_{\mathbf{p}'_j}^{(+)}. \quad (5)$$

Here, the neutrino field operator has been accordingly decomposed into discrete momentum modes, namely $\nu(t, \mathbf{x}) = \sum_{\mathbf{p}} \nu_{\mathbf{p}}^{(-)} \exp(-iEt) + \nu_{\mathbf{p}}^{(+)} \exp(iEt)$, where the negative and positive frequencies correspond to the absorption and emission of particles, respectively. The spatial dependence of field is incorporated in the field operators as $\nu_{\mathbf{p}}^{(-)} = \hat{a}_{\mathbf{p}} u(p) \exp(i\mathbf{p} \cdot \mathbf{x})$ and $\nu_{\mathbf{p}}^{(+)} = \hat{b}_{\mathbf{p}}^\dagger v(p) \exp(-i\mathbf{p} \cdot \mathbf{x})$, with \hat{a}^\dagger and \hat{b}^\dagger being the creation operators of neutrinos and antineutrinos, respectively. For Majorana neutrinos, we further have a relation $\hat{a}^\dagger = \hat{b}^\dagger$.

Contracting with external legs of ν_i and ν_j , we formally obtain $\langle \mathbf{p}'_j | \hat{j}_{ij}^\mu | \mathbf{p}_i \rangle = j_{ij}^\mu \exp[i(\mathbf{p}_i - \mathbf{p}'_j) \cdot \mathbf{x}]$. The value of the phase-independent current j_{ij}^μ will be different for Dirac and Majorana neutrinos. For Dirac neutrinos, the current simply reads

$$j_{ij}^\mu = \bar{u}_{\mathbf{p}'_j} \gamma^\mu (1 - \gamma_5) u_{\mathbf{p}_i}. \quad (6)$$

For Majorana neutrinos, the result is

$$j_{ij}^\mu = \bar{u}_{\mathbf{p}'_j} \gamma^\mu (1 - \gamma_5) u_{\mathbf{p}_i} + \bar{v}_{\mathbf{p}_i} \gamma^\mu (1 - \gamma_5) v_{\mathbf{p}'_j}, \quad (7)$$

due to two different ways of contraction. For the conversion from ν_3 to ν_1 in the NO case, the outgoing ν_1 will be ultra-relativistic because of $m_3 \gg m_1$. As a result, the interference between contributions of two different helicities in the Majorana case will be negligible. Hence, we can focus on the Dirac case, keeping in mind that the event number for the Majorana case is simply twice that of the Dirac one. Under these assumptions,

the neutrino current is simplified as

$$j_{31}^0 = +2\sqrt{2m_3 E_1} \langle \downarrow | s_3 \rangle, \quad (8)$$

$$\mathbf{j}_{31} = -2\sqrt{2m_3 E_1} \langle \downarrow | \boldsymbol{\sigma} | s_3 \rangle, \quad (9)$$

where the z -axis for the spin is defined to be aligned with \mathbf{p}_1 . The left-helical state of ν_1 is denoted by $|\downarrow\rangle$ and s_3 represents the spin of ν_3 . The expressions for the antineutrino transition are quite similar and hence skipped. In the IO case, the neutrino current for $\nu_2 \rightarrow \nu_3$ has similar expressions as Eqs. (8) and (9) with simply index replacement. However, for $\nu_2 \rightarrow \nu_1$ the outgoing neutrino will be non-relativistic, and the current becomes

$$j_{21}^0 = +2\sqrt{m_2 m_1} \langle s_1 | s_2 \rangle, \quad (10)$$

$$\mathbf{j}_{21} = -2\sqrt{m_2 m_1} \langle s_1 | \boldsymbol{\sigma} | s_2 \rangle, \quad (11)$$

where $s_{1,2}$ denotes the spin of $\nu_{1,2}$.

The essential way to calculate the fluorescence rate is to determine the Hamiltonian density for the effective neutrino-photon coupling induced by dipoles. In non-linear optics, there is a standard procedure to extract the Hamiltonian density for the electromagnetic couplings [32–34], by calculating the electric or magnetic polarization (i.e., the induced dipole moment per volume) \mathbf{P} in response to the field perturbation. The polarization reflects the strength of optical response of the medium when an external field is applied. The Hamiltonian density describing this response can be straightforwardly obtained with $\mathcal{H}_{\text{eff}} = -\mathbf{P} \cdot \boldsymbol{\mathcal{E}}$ or $\mathcal{H}_{\text{eff}} = -\mathbf{P} \cdot \boldsymbol{\mathcal{B}}$ depending on whether this polarization is electric or magnetic. Note that in medium, the field strength interacting with electric dipoles should be interpreted as the displacement field. For reference, we briefly outline the procedure for the pure electromagnetic processes in Appendix A. The effective Hamiltonian density and transition matrix for neutrino interactions can be derived in a similar manner.

A. The E1 Transition

In general, the quantum state of the system can be described as a superposition of discrete energy levels,

$$|\Psi(t)\rangle = C_g(t)|g\rangle + \sum_v C_v(t)|v\rangle, \quad (12)$$

where C_g and C_v are coefficients of the ground state and various excited states, respectively. The initial state is set to be $|\Psi_0\rangle = |g\rangle$.

As mentioned before, we assume one of the virtual states $|v\rangle$ to be dominant. For the E1 transition from $|g\rangle$ to $|v\rangle$, the relevant Hamiltonian at the atomic level is given by Eq. (3). The coefficient for $|v\rangle$ under the perturbation of neutrino fields reads

$$C_v^{(1)}(t) = \frac{G_F C_{ij}}{\sqrt{2}i} \frac{\hat{j}_{ij}^0 \mathbf{x}_{vg} \cdot (\mathbf{p}_i - \mathbf{p}'_j)}{E_{vg} + E'_j - E_i} e^{i(E_{vg} + E'_j - E_i)t}. \quad (13)$$

Note that we have temporarily ignored the damping factor in the denominator relevant for the resonance, which will be included during the rate calculation. The polarization can be obtained similar to the pure electromagnetic case, and we present the resultant effective Hamiltonian density below,

$$\begin{aligned} \mathcal{H}_{\nu\nu\gamma}^{\text{E1}} = & \frac{G_F C_{ij}}{-\sqrt{2}i} \frac{n_d [\hat{j}_{ij}^0 \mathbf{x}_{vg} \cdot (\mathbf{p}_i - \mathbf{p}'_j)] [\mathbf{d}_{gv} \cdot \boldsymbol{\mathcal{E}}(\mathbf{k})]}{E_{vg} + E'_j - E_i} \\ & \times e^{i(\omega + E'_j - E_i)t} + \text{h.c.} \end{aligned} \quad (14)$$

The temporal phase explicitly shown implies the energy conservation. Other than the temporal phase, $\mathcal{H}_{\nu\nu\gamma}^{\text{E1}}$ also carries a spatial phase in the field operators, namely $\exp[i(\mathbf{p}_i - \mathbf{p}'_j - \mathbf{k}) \cdot \mathbf{x}_r]$ as in Eq. (1). For a uniform medium, after integrating over the target volume this phase will result in the delta function $\delta^{(3)}(\mathbf{p}_i - \mathbf{p}'_j - \mathbf{k})$, which imposes the phase-matching condition (identical to the momentum conservation in vacuum) for the process to be coherent. We also highlight a scenario that the target material has a periodic profile, e.g., $n_d(\mathbf{x}) = n_d^0[1 + \cos(\mathbf{D} \cdot \mathbf{x})]$, similar to the diffraction grating in optics. In this case, the phase-matching condition will be modified according to $\delta^{(3)}(\mathbf{p}_i - \mathbf{p}'_j - \mathbf{k} \pm \mathbf{D})$, deviating from the momentum conservation in vacuum. The scattering will then induce a momentum transfer of magnitude $|\mathbf{D}|$ to the material.

The transition matrix for $\nu_i \rightarrow \nu_j \gamma$ is obtained by an integration $iT = -i \int_{-\infty}^{\infty} d^4x \langle \mathbf{p}'_j, \mathbf{k} | \mathcal{H}_{\nu\nu\gamma} | \mathbf{p}_i \rangle$. Noting $iT = i\mathcal{M} \cdot (2\pi)^4 \delta^{(4)}(p_i - p'_j - k)$, the total amplitude is extracted as

$$\mathcal{M} = \frac{G_F C_{ij}}{\sqrt{2}} \frac{n_d [\hat{j}_{ij}^0 \mathbf{x}_{vg} \cdot (\mathbf{p}_i - \mathbf{p}'_j)] [\omega \mathbf{d}_{gv} \cdot \boldsymbol{\epsilon}^*(\mathbf{k})]}{-E_{vg} - E'_j + E_i}, \quad (15)$$

where \hat{j}_{ij}^0 is given by Eq. (6), and $\boldsymbol{\epsilon}$ stands for the polarization vector of the signal photon. The relation $\boldsymbol{\mathcal{E}} = -\partial \mathbf{A} / \partial t$ has been used in obtaining the above amplitude. For the uniform material, the kinematics of the

transition is analogous to the case of the decay of non-relativistic neutrinos in vacuum, and the decay products ν_j and γ will be back-to-back. Following the standard formula, the differential decay rate in the rest frame of ν_i with respect to the photon outgoing direction is

$$\frac{d\Gamma}{d\Omega_\gamma} = \int d|\mathbf{k}| \frac{\mathbf{k}^2 |\mathcal{M}|^2}{32\pi^2 m_i E'_j \omega} \delta(\omega + E'_j - E_i). \quad (16)$$

The integration over the delta function will generate a dimensionless factor $D_k \equiv 1/[d(\omega + E'_j - E_i)/d|\mathbf{k}|]$. The actual value of D_k relies on the neutrino masses as well as the dispersion relation of photons in medium.

For $\nu_3 \rightarrow \nu_1$ with a nearly massless ν_1 in the NO case, the energy of daughter particles just takes $E'_1 = \omega = m_3/2$, assuming that the photon dispersion relation is barely modified by the medium. The value of D_k is just 2 in this case. The in-medium effect causes the energy of the signal photon to deviate from $m_3/2$ with a magnitude being material-dependent. For $\nu_2 \rightarrow \nu_1$ in the IO case, the energy of the photon is approximately $\omega \approx m_2 - m_1$. We explicitly evaluate the squared amplitude using Eq. (8) and perform the angular integration, arriving at the decay rate

$$\Gamma \approx \frac{G_F^2 |U_{ei}^* U_{ej}|^2}{2\pi e^2} \frac{f_\theta^{\text{E1}} n_d^2 |\mathbf{d}_{vg}|^4 D_k \omega |\mathbf{k}|^4}{(E_{vg} + E'_j - E_i)^2 + \Gamma_v^2/4}, \quad (17)$$

where the relation $\mathbf{x} \equiv -\mathbf{d}/e$ has been applied, and f_θ^{E1} is the form factor depending on the polarization of dipoles. The outgoing neutrino is taken to be relativistic in Eq. (17). In the case that the outgoing neutrino is non-relativistic, e.g., $\nu_2 \rightarrow \nu_1$ in IO, the expression for the rate will be reduced by a factor of two. The magnitude of f_θ^{E1} can be adjusted to be of $\mathcal{O}(1)$ by choosing a polarized material or adopting the periodic film structure even if the medium is isotropic. The damping rate Γ_v accounts for all factors that can affect the timescale of coherent accumulation of $|v\rangle$. An intrinsic contribution to Γ_v is the spontaneous decay rate of $|v\rangle$ with a typical timescale $\tau_v \sim \mathcal{O}(1 \text{ ns})$ for E1 transition. When $E_{vg} = E_i - E'_j$ is satisfied, the transition will be on resonance, and the rate will approximately be $\Gamma \sim G_F^2 n_d^2 |\mathbf{d}_{vg}|^4 |\mathbf{k}|^5 \tau_v^2$, with $|\mathbf{d}_{vg}| \sim e/(\alpha m_e)$ being the typical magnitude of the atomic or molecular electric dipole moment. The resonance enhancement also suggests that molecular materials are ideal target candidates, as their energy-level differences typically fall within the infrared range. In an ideal case that the incoming neutrino flux with a density $n_{\nu_i} \approx 112 \text{ cm}^{-3}$ (including both neutrinos and antineutrinos) can satisfy the resonance condition, the event rate $R = n_{\nu_i} V \Gamma$ in a material target of volume $V = (3 \text{ m})^3$ will roughly be given by

$$R_{\nu_3 \rightarrow \nu_1}^{\text{NO}} \sim 4 \times 10^{-8} \text{ yr}^{-1}, \quad (18)$$

$$R_{\nu_2 \rightarrow \nu_1}^{\text{IO}} \sim 7 \times 10^{-15} \text{ yr}^{-1}, \quad (19)$$

if the refractive index is unity, i.e., $|\mathbf{k}| = \omega$. Even though the scenario of $\nu_2 \rightarrow \nu_1$ in IO is not suppressed by the

smallness of U_{e3} , its rate is much smaller than that for $\nu_3 \rightarrow \nu_1$ in NO because of the tiny photon energy. However, these event numbers for the E1 transition are too small to be detectable.

B. The M1 Transition

The M1 transition is in fact preferred in our context, because its neutrino-induced current is of order one, while the current in the E1 case is suppressed by the Bohr radius. For a two-level system connected via the M1 transition, the relevant Hamiltonian describing the neutrino and photon interactions is represented by Eq. (4). In this case, the M1 transition corresponds to a flip in the electron spin. Those two spin configurations can feature different energies in the presence of couplings to the orbital angular momentum or a static magnetic field (the Zeeman effect). The coefficient of the higher state $|v\rangle$ evolves as

$$C_v^{(1)}(t) = \frac{G_F C_{ij}}{\sqrt{2}} \frac{\hat{\mathbf{j}}_{ij} \cdot \boldsymbol{\sigma}_{vg}}{E_{vg} + E'_j - E_i} e^{i(E_{vg} + E'_j - E_i)t}. \quad (20)$$

In a manner similar to the E1 transition, the effective Hamiltonian density is obtained,

$$\mathcal{H}_{\nu\nu\gamma}^{M1} = -\frac{G_F C_{ij}}{\sqrt{2}} \frac{n_d [\hat{\mathbf{j}}_{ij} \cdot \boldsymbol{\sigma}_{vg}] [\mathbf{d}_{gv} \cdot \mathcal{B}(\mathbf{k})]}{E_{vg} + E'_j - E_i} \times e^{i(\omega + E'_j - E_i)t} + \text{h.c.} \quad (21)$$

The magnetic component \mathcal{B} of the photon will contribute a value $\mathbf{k} \times \boldsymbol{\epsilon}^*$ to the amplitude.

Performing the phase space integration with Eq. (16), we find the total decay rate

$$\Gamma \approx \frac{G_F^2 |U_{ei}^* U_{ej}|^2}{2\pi} \frac{f_\theta^2 n_d^2 |\mathbf{d}_{vg}|^2 D_k}{(E_{vg} + E'_j - E_i)^2 + \Gamma_v^2/4} \frac{|\mathbf{k}|^4}{\omega}, \quad (22)$$

where $f_\theta^{M1} \sim \mathcal{O}(1)$ represents the form factor of magnetic dipoles in the material. At the resonance peak, the rate approximately has $\Gamma \sim G_F^2 n_d^2 |\mathbf{d}_{vg}|^2 |\mathbf{k}|^3 \tau_v^2$ with $|\mathbf{d}_{vg}| \sim e/m_e$ (i.e., the Bohr magneton) being the magnetic dipole moment. The coherence timescale for the M1 transition can be much longer than the E1 case due to a longer lifetime for $|v\rangle$. If we take a conservative value $\tau_v \sim \mathcal{O}(10 \text{ ns})$ and a material target of $V = (3 \text{ m})^3$, the rates on resonance will be

$$R_{\nu_3 \rightarrow \nu_1}^{\text{NO}} \sim 5 \text{ yr}^{-1}, \quad (23)$$

$$R_{\nu_2 \rightarrow \nu_1}^{\text{IO}} \sim 9 \times 10^{-4} \text{ yr}^{-1}, \quad (24)$$

assuming that the photon's dispersion relation is the same as in vacuum. The event rate for $\nu_3 \rightarrow \nu_1$ appears highly promising for those typical inputs, provided that the background can be effectively controlled. Recall that in the case of Majorana neutrinos, the event rate will be doubled, so that $R_{\nu_3 \rightarrow \nu_1}^{\text{NO}}$ can reach 10 yr^{-1} . If the signal photons can reach the material surface, mirrors and

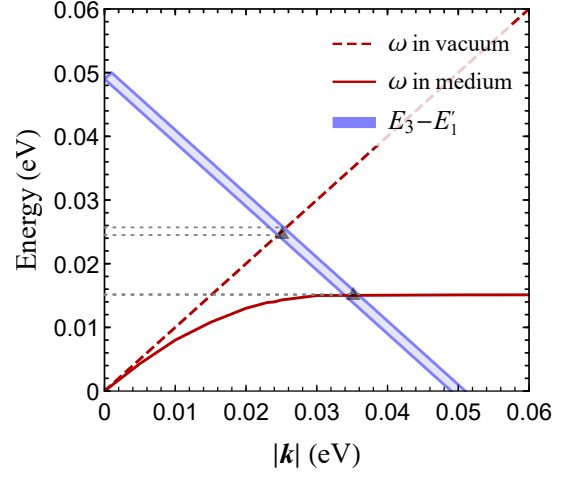


FIG. 2. The dependence curves of the photon energy ω (red) and the energy difference of neutrinos $E_3 - E'_1$ (blue) on the photon momentum $|\mathbf{k}|$ for the transition $\nu_3 \rightarrow \nu_1 \gamma$, where $m_3 = 0.05 \text{ eV}$ and $m_1 = 0 \text{ eV}$ are inputs. The shaded blue region denotes a momentum spread of order 10^{-3} eV for illustration. The intersection points marked by black triangles represent the resultant momentum and energy satisfying the conservation law.

focal planes can be used to guide them toward the infrared sensor. During their propagation, however, these photons may interact with the material lattice, resulting in dissipative phonon emission. In such cases, the emitted phonons themselves can also be detectable.

A necessary condition for achieving the rate in Eq. (23) is to have a highly monoenergetic neutrino flux that matches the energy level. Relic neutrinos with a temperature 1.95 K in the Milky Way exhibits a momentum dispersion of order $\Delta p \sim 10^{-4} \text{ eV}$, leading to a tiny energy spread of order $\Delta E_3 \approx \Delta p^2/(2m_3) \sim 10^{-6} \text{ eV}$ for the incoming non-relativistic neutrinos. The corresponding timescale of the energy spread is on the order of 1 ns. Nevertheless, the actual resonance condition $E_{vg} = E_3 - E'_1$ imposes stricter requirements, even if E_3 is already quite monoenergetic. Because the outgoing neutrino and photon are both ultra-relativistic for $\nu_3 \rightarrow \nu_1 \gamma$ with $E'_1 \approx |\mathbf{p}'_1|$ and $\omega = |\mathbf{k}|$, this momentum spread actually results in a spread of comparable magnitude $\Delta(E_3 - E'_1) \sim 10^{-4} \text{ eV}$. Thus, regardless of how the energy level is adjusted, the average decay rate seems to be capped at $\Gamma \sim G_F^2 n_d^2 |\mathbf{d}_{vg}|^2 \omega^3 / \Delta p^2$. The corresponding event rate for $\nu_3 \rightarrow \nu_1$ would be reduced to $R \sim 2 \times 10^{-6} \text{ yr}^{-1}$.

Remarkably, the impact of the momentum spread of relic neutrinos can be solved by properly adjusting photon's dispersion relation in medium. In particular, the slow-light phenomenon well recognized in modern quantum optics [36–38] can render the outgoing photon effectively non-relativistic with a reduced group velocity. By tuning photon's dispersion curve to be flat in the momentum range of interest, with $d\omega/d|\mathbf{k}| \lesssim 10^{-3}$, the energy spread $\Delta(E_3 - E'_1)$ can be controlled within

10^{-7} eV (its inverse corresponds to 10 ns). In Fig. 2, we demonstrate the dependence curves of ω and $E_3 - E'_1$ with respect to the photon momentum $|\mathbf{k}|$. The dependence of $E_3 - E'_1$ on momentum arises from the requirement of momentum conservation. The red curves represent the dispersion relation of photons in medium (solid) and in vacuum (dashed), respectively. The blue curve stands for $E_3 - E'_1$, while the shaded region denotes a momentum spread of order 10^{-3} eV, selected to be larger than the actual magnitude for demonstration. The intersection of the red and blue curves determines the actual energy satisfying the conservation law $\omega = E_3 - E'_1$. For the ω - k curve in vacuum, it is visually evident that the energy spread follows the momentum spread. In comparison, a flat dispersion curve in medium can significantly reduce the energy spread because of the tiny slope rate. Note that in Fig. 2 the dispersion curve in medium is given just for illustration. In practice, the overall shape of the curve will depend on the material. However, the primary requirement is to realize a dispersion curve that remains flat near its intersection with the blue curve. This can be achieved using many techniques such as photonic crystals in quantum optics [37]. Nevertheless, it is worth the effort in future works to develop a setup that enables dynamic engineering of the dispersion relation and scanning over the neutrino mass spectrum.

III. SUMMARY AND DISCUSSION

In analogy to nonlinear optics, neutrinos can experience the parametric fluorescence in material targets with a photon spontaneously emitted. This process is governed by the standard weak interaction of neutrinos and does not rely on any electromagnetic couplings of neutrinos in vacuum. The basic condition is no more than the presence of clean bulk material at low temperatures. The signal is an infrared photon from the dark medium environment. By coherently interacting with this material, neutrinos can develop a rather strong effective coupling to the electromagnetic field, e.g., Eqs. (14) and (21). The strength of this coupling depends largely on the detailed configurations of atomic or molecular energy levels of the material. A notable scenario is the resonance fluorescence, which occurs when the energy transferred by the neutrino matches the dipole frequency. The feasibility of using the neutrino fluorescence to detect relic neutrinos has been investigated, for which the signal photon is infrared. The event rate of $\nu_3 \rightarrow \nu_1 \gamma$ on resonance is rather considerable for the M1 transition, e.g., with $R \sim 5 \text{ yr}^{-1}$ for a target of dimension $l \sim 3 \text{ m}$. However, the challenge is presented by the intrinsic momentum dispersion of $\Delta p \sim 10^{-4} \text{ eV}$ for relic neutrinos, which normally leads to an energy dispersion of $\Delta(E_3 - E'_1) \sim 10^{-4} \text{ eV}$ and decreases the resonance enhancement. Notably, the reduction in the group velocity of photons in the relevant momentum range can help to bypass the energy spread issue.

We also remark on further possible enhancement of the event rate. The aforementioned processes involve the transition $|g\rangle \xrightarrow{\nu} |v\rangle \xrightarrow{\gamma} |g\rangle$. The transition rate under consideration is governed by the magnitudes of the neutrino and electron currents. In the case of the M1 transition, the neutrino current is of order one, while the electron current is suppressed by a factor of $\alpha^2 \sim 5 \times 10^{-5}$. Conversely, for the E1 transition, the suppression factor $m_i^2 a_0^2 \sim 10^{-10}$ appears in the neutrino current instead while the electron current is not suppressed. Normally, transitions between two energy levels cannot be of E1 (parity odd) and M1 (parity even) types at the same time because of the parity conservation. This indicates two possible mechanisms to further enlarge the rate:

- Configuration mixing. There is a potential opportunity for significant enhancement through configuration mixing between opposite parities [39]. Parity mixing renders the transition to simultaneously proceed through both E1 and M1 channels, thus evading the suppression that individually affects each mode. Configuration mixing between states of opposite parity, which implies parity violation, can be achieved with many methods, such as the Stark effect in the presence of an external electric field. The Stark effect has been extensively employed in experiments probing atomic parity violation [40, 41], owing to its ability to induce sizable parity mixing. For a maximal enhancement, it is crucial to make the parity mixing as large as possible, ideally of order one. Achieving such strong mixing could yield an overall enhancement factor on the order of $1/\alpha^2 \sim 10^4$ on top of the original rate in Eq. (23).
- Superradiance of a Λ -like system. One possible way to avoid the suppression in the E1/M1 transition is to make neutrinos and photons interact with different levels. Let us denote the initial and final levels of the transition as $|e\rangle$ and $|g\rangle$ (vice versa), respectively. Then, the process induced by relic neutrinos will be $\nu_i + |e\rangle \rightarrow \nu_j + \gamma_S + |g\rangle$. In a Λ -like system, the transition proceeds as $|e\rangle \xrightarrow{\nu} |v\rangle \xrightarrow{\gamma} |g\rangle$ through the intermediate state $|v\rangle$. We further assume the successive transitions are of M1 and E1 types, respectively, with the neutrino coupling to the first transition and the photon coupling to the second. Then, the problem is how coherence can be maintained if the initial and final levels are different. The benefit of superradiance is that coherence is kept even if the atomic or molecular state has been altered by the scattering. Superradiance takes place when the ensemble is manipulated into a superposition of ground and excited states $|\psi\rangle$. The coherence of the ensemble will be measured by a factor of order one, $\rho_{eg} \equiv \langle e|\psi\rangle\langle\psi|g\rangle$. The superradiance mechanism itself has already been considered as an enhancement method to probe neutrino physics [42–50], including the absolute scale of neutrino masses first proposed in Ref. [51] as well as relic neutrinos [52, 53].

The detection of relic neutrinos can also help to pin down basic neutrino properties, such as the absolute scale of neutrino masses and the Majorana nature. Besides relic neutrinos, the parametric fluorescence mechanism explored in the present work may also be applied to the atomic detection of dark matter [54–58] and other monoenergetic neutrino fluxes such as Mössbauer neutrinos. For example, in the environment of atomic or molecular dipoles, axion dark matter can feature a resonantly enhanced rate of spontaneous decay into two photons, i.e., $a \rightarrow \gamma\gamma$, similar to the original SPDC process. Since the main purpose of this work is to put forward a promising direction for relic neutrino detection, its ultimate experimental realization will be addressed in future works, which requires a dedicated search for suitable atomic or molecular candidates in the context of modern technologies achievable in quantum optics.

ACKNOWLEDGMENTS

This work is supported in part by the “CUG Scholar” Scientific Research Funds at China University of Geosciences (Wuhan) under project No. 2024014, and by the National Natural Science Foundation of China under grant No. 12475113 and grant No. 12405130.

Appendix A: Pure Electromagnetic Processes

It will be instructive to review the pure electromagnetic processes in nonlinear optics [32] and outline the necessary procedure in accordance with the notations of the present work. For a dielectric medium, the polarization can be formally expanded as power series of the electric field in the weak-field approximation,

$$P_i \supset \chi_{ij}^{(1)} \mathcal{E}_j + \chi_{ijk}^{(2)} \mathcal{E}_j \mathcal{E}_k + \chi_{ijkl}^{(3)} \mathcal{E}_j \mathcal{E}_k \mathcal{E}_l + \dots, \quad (\text{A1})$$

where $\chi^{(1)}$ is known as the linear susceptibility of the medium, and $\chi^{(i)}$ (for $i > 1$) denotes the nonlinear susceptibilities. The linear susceptibility, corresponding to the diagram in Fig. (3a), is connected to the refractive index through $n = \sqrt{1 + \text{Re}(\chi^{(1)})}$. The SPDC process is controlled by $\chi^{(2)}$ describing three photon couplings, which is a second-order process. Depicted by Fig. (3b), SPDC requires a three-level system, for which different levels are connected via the electric-dipole interaction $H_d = -\mathbf{d} \cdot \mathbf{E}$.

Suppose that the electromagnetic field is composed of plane waves with several discrete frequencies, $\mathbf{E}(t, \mathbf{x}) = \sum_i \mathbf{E}(\mathbf{k}_i) \cdot \exp(-i\omega_i t)$ including both the positive and negative frequencies. Note that the spatial phase is implicitly incorporated in $\mathbf{E}(\mathbf{k}_i)$. Under the perturbation of this field, the level coefficient of the virtual state $|\mathbf{v}\rangle$

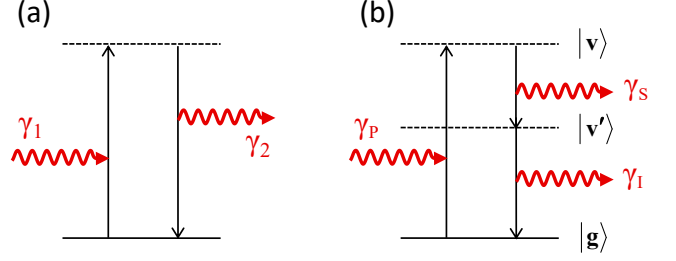


FIG. 3. The fundamental diagrams for the generation of additional electromagnetic couplings by coherently scattering with atomic/molecular energy levels: (a) the coupling $\gamma\gamma$ corresponding to the linear electric susceptibility which changes the refractive index of lights; (b) the coupling $\gamma\gamma\gamma$ corresponding to the nonlinear electric susceptibility that induces the down conversion of pumping photons. The ground and virtual states are denoted by $|\mathbf{g}\rangle$ and $|\mathbf{v}\rangle$ (or $|\mathbf{v}'\rangle$), respectively. Those scatterings are coherent because the transition returns back to the ground state via the short-lived intermediate state.

to the first order evolve as

$$C_v^{(1)}(t) = -i \int_{-\infty}^t d\tilde{t} \langle \mathbf{v} | H_d(\tilde{t}) | \mathbf{g} \rangle \\ = \sum_i \frac{\mathbf{d}_{vg} \cdot \mathbf{E}(\omega_i)}{E_{vg} - \omega_i} e^{i(E_{vg} - \omega_i)t}, \quad (\text{A2})$$

where we have neglected the rapidly oscillating term when the time integration approaches infinity. The linear polarization per radiant $\langle \mathbf{d} \rangle = \sum_v C_v^{(1)} \langle \mathbf{g} | \mathbf{d} | \mathbf{v} \rangle + C_v^{(1)*} \langle \mathbf{v} | \mathbf{d} | \mathbf{g} \rangle$ summing over all the virtual states has the following explicit expression

$$\langle \mathbf{d} \rangle^{(1)} = \sum_{i,v} \frac{\mathbf{d}_{gv} [\mathbf{d}_{vg} \cdot \mathbf{E}(\omega_i)]}{E_{vg} - \omega_i} e^{-i\omega_i t} + \text{h.c.}, \quad (\text{A3})$$

The polarization per unit volume then reads $\mathbf{P}^{(1)} = n_d \langle \mathbf{d} \rangle^{(1)}$, where $n_d \sim N_A \text{ cm}^{-3}$ represents the density of dipoles. Diagrammatically, this first-order polarization stems from the transition process $|\mathbf{g}\rangle \xrightarrow{\gamma} |\mathbf{v}\rangle \xrightarrow{\gamma} |\mathbf{g}\rangle$ as in Fig. (3b). The first term (or its hermitian conjugate) of Eq. (A3) corresponds to the scenario where γ_1 (or γ_2) is taken as the primary perturbation. Using $\mathcal{H}_{2\gamma}^{(1)} = -\mathbf{P}^{(1)} \cdot \mathbf{E}(t, \mathbf{x})$, the Hamiltonian density due to the medium effect reads

$$\mathcal{H}_{2\gamma}^{(1)} = \sum_{i,j,v} \frac{n_d [\mathbf{d}_{gv} \cdot \mathbf{E}(\mathbf{k}_j)] [\mathbf{d}_{vg} \cdot \mathbf{E}(\mathbf{k}_i)]}{\omega_i - E_{vg}} e^{-i(\omega_i + \omega_j)t} \\ + \text{h.c.}, \quad (\text{A4})$$

which couples the electric components of two photons.

Let us now proceed to the second-order process. The second-order coefficients under the perturbation can be

obtained by a further iteration as

$$C_v^{(2)}(t) = -i \int_{-\infty}^t d\tilde{t} \sum_{v'} \langle v | H_d(\tilde{t}) | v' \rangle C_{v'}^{(1)}(\tilde{t}) \quad (\text{A5})$$

$$= \sum_{i,j,v'} \frac{[\mathbf{d}_{vv'} \cdot \boldsymbol{\mathcal{E}}(\omega_j)] [\mathbf{d}_{v'g} \cdot \boldsymbol{\mathcal{E}}(\omega_i)]}{(E_{vg} - \omega_i - \omega_j)(E_{v'g} - \omega_i)} e^{i(E_{vg} - \omega_i - \omega_j)t}.$$

Similar to the first-order case, the corresponding polarization per volume has the following expression

$$P^{(2)} = n_d \left(\sum_v C_v^{(2)} \langle g | \mathbf{d} | v \rangle + C_v^{(2)*} \langle v | \mathbf{d} | g \rangle + \sum_{v,v'} C_v^{(1)} C_{v'}^{(1)*} \langle v' | \mathbf{d} | v \rangle \right). \quad (\text{A6})$$

The second-order Hamiltonian density can be straightforwardly obtained with $\mathcal{H}_{3\gamma}^{(2)} = -\mathbf{P}^{(2)} \cdot \boldsymbol{\mathcal{E}}(t, \mathbf{x})$. However, the result of the Hamiltonian for the $\gamma\gamma\gamma$ coupling is quite tedious and involves many permutations of photon fields, and thus we do not present the explicit expression here. With those results, one is able to calculate the rate for the SPDC process $\gamma_P \rightarrow \gamma_S + \gamma_I$, after the material has been specified.

-
- [1] **Planck**, N. Aghanim *et al.*, “*Planck 2018 results. VI. Cosmological parameters*,” *Astron. Astrophys.* **641** (2020) A6, [arXiv:1807.06209](#). [Erratum: *Astron. Astrophys.* 652, C4 (2021)].
 - [2] S. Weinberg, “*Universal Neutrino Degeneracy*,” *Phys. Rev.* **128** (1962) 1457–1473.
 - [3] **PTOLEMY**, E. Baracchini *et al.*, “*PTOLEMY: A Proposal for Thermal Relic Detection of Massive Neutrinos and Directional Detection of MeV Dark Matter*,” [arXiv:1808.01892](#).
 - [4] **PTOLEMY**, M. G. Betti *et al.*, “*Neutrino physics with the PTOLEMY project: active neutrino properties and the light sterile case*,” *JCAP* **07** (2019) 047, [arXiv:1902.05508](#).
 - [5] **PTOLEMY**, A. Apponi *et al.*, “*Heisenberg’s uncertainty principle in the PTOLEMY project: A theory update*,” *Phys. Rev. D* **106** (2022) no. 5, 053002, [arXiv:2203.11228](#).
 - [6] Y. Cheipesh, V. Cheianov, and A. Boyarsky, “*Navigating the pitfalls of relic neutrino detection*,” *Phys. Rev. D* **104** (2021) no. 11, 116004, [arXiv:2101.10069](#).
 - [7] Y. Cheipesh, I. Ridkokasha, V. Cheianov, and A. Boyarsky, “*Can we really detect relic neutrinos?*,” *SciPost Phys. Proc.* **12** (2023) 042.
 - [8] R. Opher, “*Coherent scattering of cosmic neutrinos*,” *Astron. Astrophys.* **37** (1974) no. 1, 135–137.
 - [9] R. R. Lewis, “*Coherent Detector for Low-energy Neutrinos*,” *Phys. Rev. D* **21** (1980) 663.
 - [10] Y. B. Zeldovich and M. Y. Khlopov, “*The Neutrino Mass in Elementary Particle Physics and in Big Bang Cosmology*,” *Sov. Phys. Usp.* **24** (1981) 755–774.
 - [11] N. Cabibbo and L. Maiani, “*The Vanishing of Order G Mechanical Effects of Cosmic Massive Neutrinos on Bulk Matter*,” *Phys. Lett. B* **114** (1982) 115–117.
 - [12] B. F. Shvartsman, V. B. Braginsky, S. S. Gershtein, Y. B. Zeldovich, and M. Y. Khlopov, “*Possibility of Detecting Relic Massive Neutrinos*,” *JETP Lett.* **36** (1982) 277–279.
 - [13] P. Langacker, J. P. Leveille, and J. Sheiman, “*On the Detection of Cosmological Neutrinos by Coherent Scattering*,” *Phys. Rev. D* **27** (1983) 1228.
 - [14] P. F. Smith and J. D. Lewin, “*Coherent Interaction of Galactic Neutrinos with Material Targets*,” *Phys. Lett. B* **127** (1983) 185–190.
 - [15] R. R. Lewis, “*Radiation Pressure of Neutrinos in Refracting Media*,” *Phys. Rev. D* **35** (1987) 2134–2141.
 - [16] A. Loeb and G. D. Starkman, “*A Detector for the Cosmic Neutrino Background*,” *Nucl. Phys. B Proc. Suppl.* **19** (1991) 241–250.
 - [17] I. Ferreras and I. Wasserman, “*Feasibility of observing mechanical effects of cosmological neutrinos*,” *Phys. Rev. D* **52** (1995) 5459–5479.
 - [18] C. Hagmann, “*Cosmic neutrinos and their detection*,” in *American Physical Society (APS) Meeting of the Division of Particles and Fields (DPF 99)*. 1, 1999. [arXiv:astro-ph/9905258](#).
 - [19] G. Duda, G. Gelmini, and S. Nussinov, “*Expected signals in relic neutrino detectors*,” *Phys. Rev. D* **64** (2001) 122001, [arXiv:hep-ph/0107027](#).
 - [20] G. B. Gelmini, “*Prospect for relic neutrino searches*,” *Phys. Scripta T* **121** (2005) 131–136, [arXiv:hep-ph/0412305](#).
 - [21] A. Ringwald, “*Prospects for the direct detection of the cosmic neutrino background*,” *Nucl. Phys. A* **827** (2009) 501C–506C, [arXiv:0901.1529](#).
 - [22] P. Vogel, “*How difficult it would be to detect cosmic neutrino background?*,” *AIP Conf. Proc.* **1666** (2015) no. 1, 140003.
 - [23] V. Domcke and M. Spinrath, “*Detection prospects for the Cosmic Neutrino Background using laser interferometers*,” *JCAP* **06** (2017) 055, [arXiv:1703.08629](#).
 - [24] J. D. Shergold, “*Updated detection prospects for relic neutrinos using coherent scattering*,” *JCAP* **11** (2021) no. 11, 052, [arXiv:2109.07482](#).
 - [25] A. Ruzi, S. Qian, T. Yang, and Q. Li, “*Low Energy Neutrino and Mass Dark Matter Detection Using Freely Falling Atoms*,” [arXiv:2302.09874](#).
 - [26] **JUNO**, F. An *et al.*, “*Neutrino Physics with JUNO*,” *J. Phys. G* **43** (2016) no. 3, 030401, [arXiv:1507.05613](#).
 - [27] **JUNO**, A. Abusleme *et al.*, “*Potential to identify neutrino mass ordering with reactor antineutrinos at JUNO*,” *Chin. Phys. C* **49** (2025) no. 3, 033104,

- arXiv:2405.18008.
- [28] K. Homma, Y. Kiritu, T. Miyamaru, T. Hasada, and A. Kodama, “Opening a meV mass window for axionlike particles with a microwave-laser-mixed stimulated resonant photon collider,” *Phys. Rev. D* **110** (2024) no. 9, 092017, arXiv:2405.03577.
 - [29] S. H. Kim et al., “Development of Superconducting Tunnel Junction Far-Infrared Photon Detector for Cosmic Background Neutrino Decay Search - COBAND experiment,” *PoS ICHEP2018* (2019) 427.
 - [30] J. J. A. Baselmans et al., “A kilo-pixel imaging system for future space based far-infrared observatories using microwave kinetic inductance detectors,” *Astron. Astrophys.* **601** (2017) A89, arXiv:1609.01952.
 - [31] P. M. Echternach, B. J. Pepper, T. Reck, and C. M. Bradford, “Single photon detection of 1.5 THz radiation with the quantum capacitance detector,” *Nature Astronomy* **2** (Nov., 2018) 90–97.
 - [32] R. W. Boyd, *Nonlinear Optics, Third Edition*. Academic Press, Inc., USA, 3rd ed., 2008.
 - [33] D. N. Klyshko, *Photons and Nonlinear Optics*. 1988.
 - [34] P. N. Butcher and D. Cotter, *The Elements of Nonlinear Optics*. Cambridge Studies in Modern Optics. Cambridge University Press, 1990.
 - [35] Y. Shih, “Entangled biphoton source - property and preparation,” *Reports on Progress in Physics* **66** (may, 2003) 1009. <https://dx.doi.org/10.1088/0034-4885/66/6/203>.
 - [36] L. V. Hau, S. E. Harris, Z. Dutton, and C. H. Behroozi, “Light speed reduction to 17 metres per second in an ultracold atomic gas,” *Nature* **397** (1999) no. 6720, 594–598.
 - [37] R. S. T. Jacob B. Khurgin, *Slow Light: Science and Applications*. Optical Science and Engineering. CRC Press, 1 ed., 2008.
 - [38] J. B. Khurgin, “Slow light in various media: a tutorial,” *Adv. Opt. Photon.* **2** (Sep, 2010) 287–318. <https://opg.optica.org/aop/abstract.cfm?URI=aop-2-3-287>.
 - [39] B. Bransden and C. Joachain, *Physics of Atoms and Molecules*. Dorling Kindersley Pvt Ltd, 2006.
 - [40] M. A. Bouchiat and C. Bouchiat, “Parity Violation Induced by Weak Neutral Currents in Atomic Physics. Part 2,” *J. Phys. (France)* **36** (1975) 493–509.
 - [41] M. Bouchiat, J. Guena, L. Hunter, and L. Pottier, “Observation of a parity violation in cesium,” *Physics Letters B* **117** (1982) no. 5, 358–364. <https://www.sciencedirect.com/science/article/pii/0370269382907365>.
 - [42] A. Fukumi et al., “Neutrino Spectroscopy with Atoms and Molecules,” *PTEP* **2012** (2012) 04D002, arXiv:1211.4904.
 - [43] M. Yoshimura, N. Sasao, and M. Tanaka, “Dynamics of paired superradiance,” *Phys. Rev. A* **86** (2012) 013812, arXiv:1203.5394.
 - [44] D. N. Dinh, S. T. Petcov, N. Sasao, M. Tanaka, and M. Yoshimura, “Observables in Neutrino Mass Spectroscopy Using Atoms,” *Phys. Lett. B* **719** (2013) 154–163, arXiv:1209.4808.
 - [45] N. Song, R. Boyero Garcia, J. J. Gomez-Cadenas, M. C. Gonzalez-Garcia, A. Peralta Conde, and J. Taron, “Conditions for Statistical Determination of the Neutrino Mass Spectrum in Radiative Emission of Neutrino Pairs in Atoms,” *Phys. Rev. D* **93** (2016) no. 1, 013020, arXiv:1510.00421.
 - [46] J. Zhang and S. Zhou, “Improved Statistical Determination of Absolute Neutrino Masses via Radiative Emission of Neutrino Pairs from Atoms,” *Phys. Rev. D* **93** (2016) no. 11, 113020, arXiv:1604.08008.
 - [47] G.-Y. Huang, N. Sasao, Z.-Z. Xing, and M. Yoshimura, “Testing unitarity of the 3×3 neutrino mixing matrix in an atomic system,” *Int. J. Mod. Phys. A* **35** (2020) no. 01, 2050004, arXiv:1904.10366.
 - [48] S.-F. Ge and P. Pasquini, “Probing light mediators in the radiative emission of neutrino pair,” *Eur. Phys. J. C* **82** (2022) no. 3, 208, arXiv:2110.03510.
 - [49] S.-F. Ge and P. Pasquini, “Unique probe of neutrino electromagnetic moments with radiative pair emission,” *Phys. Lett. B* **841** (2023) 137911, arXiv:2206.11717.
 - [50] S.-F. Ge and P. Pasquini, “Disentangle neutrino electromagnetic properties with atomic radiative pair emission,” *JHEP* **12** (2023) 083, arXiv:2306.12953.
 - [51] M. Yoshimura, “Neutrino Pair Emission from Excited Atoms,” *Phys. Rev. D* **75** (2007) 113007, arXiv:hep-ph/0611362.
 - [52] M. Yoshimura, N. Sasao, and M. Tanaka, “Experimental method of detecting relic neutrino by atomic de-excitation,” *Phys. Rev. D* **91** (2015) no. 6, 063516, arXiv:1409.3648.
 - [53] A. Arvanitaki, S. Dimopoulos, and M. Galanis, “Superradiant interactions of the cosmic neutrino background, axions, dark matter, and reactor neutrinos,” *Phys. Rev. D* **111** (2025) no. 5, 055015, arXiv:2408.04021.
 - [54] M. S. Safronova, D. Budker, D. DeMille, D. F. J. Kimball, A. Derevianko, and C. W. Clark, “Search for New Physics with Atoms and Molecules,” *Rev. Mod. Phys.* **90** (2018) no. 2, 025008, arXiv:1710.01833.
 - [55] A. Arvanitaki, S. Dimopoulos, and K. Van Tilburg, “Resonant absorption of bosonic dark matter in molecules,” *Phys. Rev. X* **8** (2018) no. 4, 041001, arXiv:1709.05354.
 - [56] G.-Y. Huang and S. Zhou, “Probing Cosmic Axions through Resonant Emission and Absorption in Atomic Systems with Superradiance,” *Phys. Rev. D* **100** (2019) no. 3, 035010, arXiv:1905.00367.
 - [57] A. Bhoonah, J. Bramante, and N. Song, “Superradiant Searches for Dark Photons in Two Stage Atomic Transitions,” *Phys. Rev. D* **101** (2020) no. 5, 055040, arXiv:1909.07387.
 - [58] M. Bauer, J. Perez-Soler, and J. D. Shergold, “Generalised hydrogen interactions with CINCO: a window to new physics,” *JHEP* **10** (2024) 176, arXiv:2407.12913.